

DOI: 10.1002/cmdc.201402015

Design, Synthesis, and Biological Evaluation of 1,3-Diarylpropenones as Dual Inhibitors of HIV-1 Reverse Transcriptase

Rita Meleddu,^[a] Valeria Cannas,^[b] Simona Distinto,^{*[a]} Giorgia Sarais,^[a] Claudia Del Vecchio,^[c] Francesca Esposito,^[b] Giulia Bianco,^[a] Angela Corona,^[b] Filippo Cottiglia,^[a] Stefano Alcaro,^[d] Cristina Parolin,^[e] Anna Artese,^[d] Daniela Scalise,^[d] Massimo Fresta,^[d] Antonella Arridu,^[a] Francesco Ortuso,^[d] Elias Maccioni,^{*[a]} and Enzo Tramontano^[b]

A small library of 1,3-diarylpropenones was designed and synthesized as dual inhibitors of both HIV-1 reverse transcriptase (RT) DNA polymerase (DP) and ribonuclease H (RNase H) associated functions. Compounds were assayed on these enzyme activities, which highlighted dual inhibition properties in the low-micromolar range. Interestingly, mutations in the non-nu-

cleoside RT inhibitor binding pocket strongly affected RNase H inhibition by the propenone derivatives without decreasing their capacity to inhibit DP activity, which suggests long-range RT structural effects. Biochemical and computational studies indicated that the propenone derivatives bind two different interdependent allosteric pockets.

Introduction

The design of multiple-acting ligands has become a fascinating challenge for the therapy of diseases with multifarious pathological mechanisms such as human immunodeficiency virus (HIV) and acquired immunodeficiency syndrome (AIDS).^[1] The inhibition of multiple targets with a single molecule could improve patient compliance and decrease the occurrence of drug resistance.^[2]

Since the identification of HIV-1 as the causative agent of AIDS, more than 20 antiretroviral drugs targeting different steps of the HIV replication cycle have been approved for the clinical treatment of HIV-infected patients.^[3] Among these, one of the most attractive and explored targets is HIV-1 reverse

transcriptase (RT), which is responsible for retrotranscription. This process converts the viral single-stranded RNA genome into integration-competent double-stranded DNA through the formation of an RNA/DNA hybrid intermediate. RT consists of two subunits of different length, p66 and p51, which are combined in a stable asymmetric heterodimer.^[4]

Currently, two classes of RT inhibitors (RTIs) are included in approved combination treatments used for HIV-1 handling, namely, nucleoside/nucleotide RT inhibitors (NRTIs/NtRTIs) and non-nucleoside RT inhibitors (NNRTIs).^[3,5] Notably, despite its critical relevance for the HIV life cycle,^[6] no drugs are clinically available for the inhibition of the RT-associated RNase H function, even though some RNase H inhibitors have recently been designed and studied.^[7] Most of the RNase H inhibitors identified so far chelate divalent metal ions [magnesium(II), Mg^{II}] that are coordinated in the active site by the catalytic residues D443, E478, D498, and D549. These compounds, however, show toxicity as a result of the lack of specific binding.^[8] Interestingly, it was recently reported that some hydrazones,^[9] naphthyridinone,^[8c] and anthraquinone derivatives^[10] inhibit the HIV-1 RNase H function by recognizing an allosteric pocket located between the polymerase catalytic region and the NNRTI binding pocket (NNRTIBP), which is 50 Å away from the RNase H catalytic site, and by directly communicating with the NNRTIBP.^[9]

Clearly, the development of compounds that inhibit both RT-associated RNA-dependent DNA polymerase (RDDP) and RNase H activities would have several advantages that would lead to a complete block of RT functions, new favorable drug-resistance profiles, a decrease in the use of drug combinations, and a reduction in toxic side effects. However, almost all classes of RTIs are selective toward one of the two main RT-as-

[a] Dr. R. Meleddu, Dr. S. Distinto, Dr. G. Sarais, Dr. G. Bianco, Dr. F. Cottiglia, Dr. A. Arridu, Prof. E. Maccioni
Department of Life and Environmental Sciences
University of Cagliari, Via Ospedale 72, 09124 Cagliari (Italy)
E-mail: s.distinto@unica.it
maccione@unica.it

[b] Dr. V. Cannas, Dr. F. Esposito, Dr. A. Corona, Prof. E. Tramontano
Department of Life and Environmental Sciences
University of Cagliari, Cittadella Universitaria di Monserrato, SS554
09042 Monserrato, Cagliari (Italy)

[c] Dr. C. Del Vecchio
Department of Molecular Medicine
University of Padua, Via Gabelli, 63, 35121 Padua (Italy)

[d] Prof. S. Alcaro, Dr. A. Artese, Dr. D. Scalise, Prof. M. Fresta, Dr. F. Ortuso
Dipartimento di Scienze della Salute
Università Magna Graecia di Catanzaro, Campus "S. Venuta"
Viale Europa, 88100 Catanzaro (Italy)

[e] Prof. C. Parolin
Department of Biology
University of Padua, via U. Bassi 58/b, 35121 Padua (Italy)

 Supporting information for this article is available on the WWW under <http://dx.doi.org/10.1002/cmdc.201402015>.

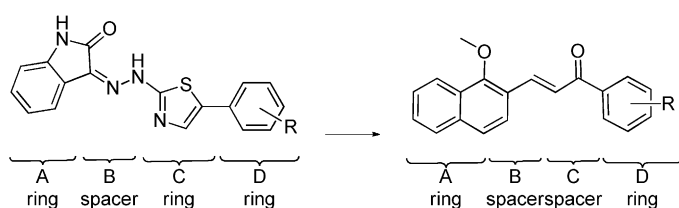
sociated activities^[3,5,7d] and only a few are active on both of them.^[9–11]

Recently, we reported the identification of HIV-1 RT single-site dual inhibitors (SSDIs) by a combined shape-, 2D-fingerprint-, and pharmacophore-based virtual screening approach.^[12] Pursuing the strategy of developing new anti-HIV inhibitors, we designed and synthesized a series of 3-(1-methoxynaphthalen-2-yl)-1-arylprop-2-en-1-one derivatives, evaluated their activity against both HIV-1 RT-associated functions, and characterized their mechanism of action.

Results and Discussion

Design and synthesis of new compounds

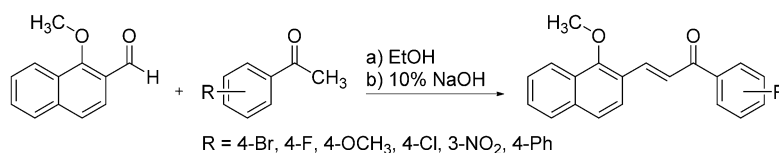
On the basis of compound **46** (compound numbering in Ref. [12]) as a hit compound (HC) for the dual inhibition of both associated HIV-1 RTs, we applied bioisosteric substitutions for the identification of novel compounds. Bioisosterism demonstrated to be a valid approach to navigate the chemical space to optimize the biological performance of small molecules.^[13] The HC should have a completely well-known chemical structure and possess an equally well-known mechanism of action, if possible at the level of topographic interaction with the receptor, including knowledge of its complete pharmacophore model. Docking analysis of **46** was performed not only toward the wild-type (WT) enzyme, but also versus the most common mutants (i.e., Y181C, K103N). Interestingly, a common binding feature in all of the theoretical ligand–enzyme complexes is the formation of a π – π interaction between the indolinone ring and W229, a highly conserved residue.^[14] The main HC structural features are an aromatic portion (A ring), a hydrazine spacer (B), and



Scheme 1. Schematic representation of HC **46** and new derivatives.

a thiazole ring (C) bearing a second aromatic ring (D) at the 4-position (Scheme 1).

3-(1-Methoxynaphthalen-2-yl)-1-arylprop-2-en-1-one derivatives were designed according to this pharmacophoric scheme. The indolinone ring was replaced by the 1-methoxynaphthalene moiety, the hydrazine spacer was substituted by a vinyl group, and the thiazole was replaced by the bioisosteric



Scheme 2. General synthetic pathway to compounds of this study.

carbonyl feature.^[15] As expected, the entire series had the *E* configuration according to the coupling constants for the proton on the C=C bond. All compounds were synthesized by Claisen–Schmidt condensation (Scheme 2). Briefly, in a general procedure, the appropriate methyl aryl ketone (1 equiv) was dissolved in ethanol and a solution of 10% aqueous NaOH was added dropwise. 1-Methoxy-2-naphthaldehyde (2 equiv) was added to the basic solution under vigorous stirring at room temperature. The mixture was stirred for 24 h, and the formed solid was filtered, washed with water, and crystallized from water/ethanol. The structures of all the derivatives were further confirmed by mass spectrometry (Figure S1, Supporting Information). All compounds exhibited a similar fragmentation pattern, which led to common sets of characteristic and well-detectable fragment ions (Table 1).

Table 1. Representative fragment ions of compounds EMAC2000–2005 with their relative abundance.

Compd	[M ⁺]	Molecular and fragment ions a–d [m/z] (%) ^[a]			
		a	b	c	d
EMAC2000	367 (100)	335 (57.7)	285 (57.7)	241 (46.2)	211 (19.2)
EMAC2001	307 (83.7)	285 (100)	275 (36.7)	241 (61.2)	211 (10.4)
EMAC2002	319 (100)	287 (79.3)	285 (14.9)	241 (6.9)	211 (26.4)
EMAC2003	323 (100)	291 (77.1)	285 (37.1)	285 (37.1)	211 (14.3)
EMAC2004	334 (80)	302 (100)	285 (17.2)	241 (16.0)	211 (8.0)
EMAC2005	365 (100)	333 (65.9)	285 (34.1)	241 (27.3)	211 (18.2)

[a] See Supporting Information Figure S1.

Evaluation of 1,3-diarylpropenones on the functions of HIV-1 RT

The efficacy of the synthesized 1,3-diarylpropenone derivatives on both of the RT-associated functions was measured in biochemical assays by using RDS1643^[8b] and efavirenz as positive controls (Table 2). Interestingly, the most potent inhibitors were EMAC2005 and EMAC2002.

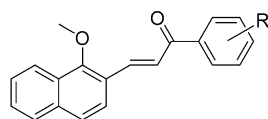
Preliminary structure–activity relationship analysis showed that although the RDDP activity was not affected by variation of the substituent at the 4-position of the D ring, the RNase H activity was strongly influenced. In particular, bulky and strongly/weakly activating groups (e.g., methoxy and phenyl) were preferred with respect to deactivating substituents (e.g., halogens). The introduction of a nitro group at the 3-position of the D ring was slightly more tolerated, probably because of its minor conjugative electron-withdrawing effect.

Next, the activity of the compounds was tested on the replication ability of HIV-1 in a single round of infection in Jurkat

Table 2. HIV-1 RT-associated activity inhibition by the 1,3-diarylpropene derivatives.

Compd	R	IC ₅₀ [μM]	
		RNase H ^[a]	RDDP ^[b]
EMAC2000	4-Br	47 ± 1	6 ± 1
EMAC2001	4-F	23 ± 3	5 ± 1
EMAC2002	4-OCH ₃	9 ± 2	6 ± 2
EMAC2003	4-Cl	76 ± 11	5 ± 1
EMAC2004	3-NO ₂	31 ± 4	5 ± 1
EMAC2005	4-Ph	6 ± 2	4 ± 1
RDS1643		13	13 ± 3
efavirenz		> 10	> 10

[a] Compound concentration required to inhibit HIV-1 RT-associated RNase H activity by 50%. [b] Compound concentration required to inhibit HIV-1 RT-associated RDDP activity by 50%.



cells. Given that the CC₅₀ values (cytotoxic concentration for 50% of cells) ranged between 3 and 15 μM, compound concentrations were set at 10 μM for EMAC2000; 5, 0.5, and 0.05 μM for EMAC2000 and EMAC2003; and 0.5 and 0.05 μM for EMAC2004 and EMAC2005. All compounds were not able to inhibit HIV-1 replication within these experimental conditions (Figure 1). Thus, we performed in vitro permeability assays to assess if a reduced or absent transmembrane permeation could explain these results.

Biochemical characterization of the mechanism of HIV-1 RT inhibition by EMAC2005

Several classes of HIV-1 RNase H have been reported, and in general, they act by chelating the Mg^{II} ions within the active

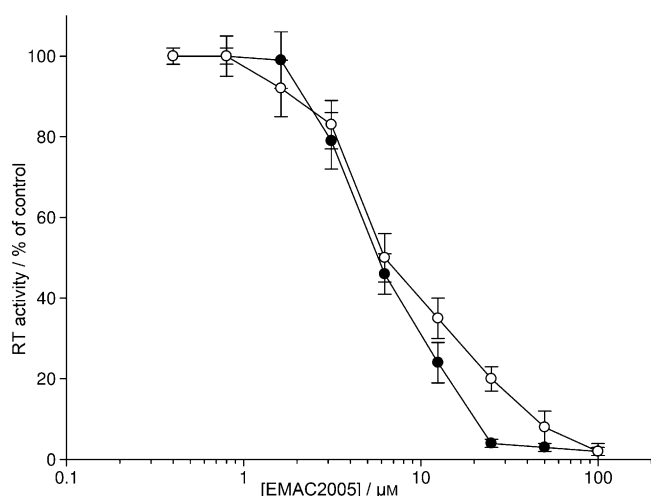


Figure 1. Inhibition of HIV-1 RT-associated RDDP (●) and RNase H (○) functions by EMAC2005; data represent mean values ± SD from three independent determinations.

site, which is essential for enzyme function. To verify the possibility that 1-(4-biphenyl)-3-(1-methoxynaphthalen-2-yl)prop-2-en-1-one (EMAC2005) could chelate the divalent ions in the RNase H catalytic site, we determined its absorbance spectra in the absence and presence of MgCl₂, but we did not observe any differences (data not shown).

Subsequently, we further investigated if EMAC2005 and the diketo acid derivative RDS1643, an RNase H catalytic site inhibitor,^[8b] were able to simultaneously bind to the RT. Such an evaluation was performed by means of the Yonetani-revised Yonetani–Theorell model, which allows the competition between two inhibitors of a certain enzyme for the same binding site or two non-overlapping binding sites to be determined. In this revised model, the plot of the inverse of the reaction velocity (1/V) observed in the presence of various concentrations of the first inhibitor, in the absence or in the contemporaneous presence of the second inhibitor, leads to a series of lines that are parallel if the two inhibitors compete for the same binding site or a series of lines that intersect if the inhibitors bind to different enzyme sites.^[16]

Therefore, the HIV-1 RT RNase H activity was measured in the presence of increasing concentrations of both EMAC2005 and RDS1643 and analyzed with the Yonetani–Theorell plot (Figure 2). The results showed that the slope of the plots of 1/V versus the EMAC2005 concentration decreased at increasing RDS1643 concentrations, which confirmed that the two compounds were not kinetically mutually exclusive. Overall, these data support the hypothesis that EMAC2005 does not bind to the HIV-1 RNase H catalytic site.

Next, we evaluated the effects of EMAC2005 on K103N- and Y181C-mutated RTs involved in NNRTI resistance (Table 3). The results showed that upon testing K103N RT, EMAC2005 was 10-fold less potent on the RNase H. On the contrary, no influence of K103N mutation on the RDDP activity was observed. In the case of Y181C mutation, a more dramatic effect relative to that observed for K103N was observed: the activity toward

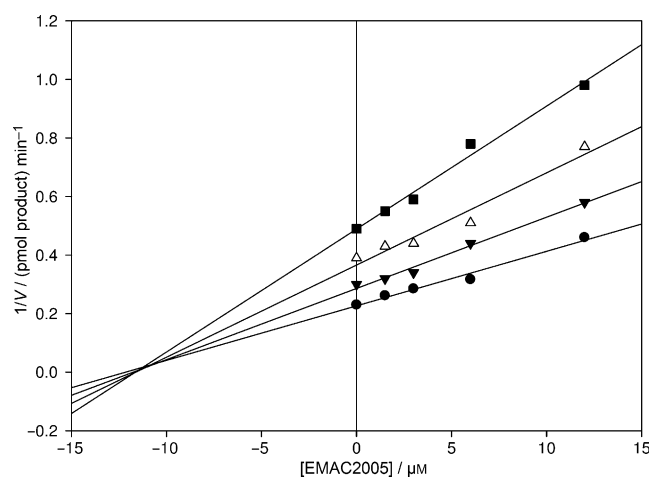


Figure 2. Yonetani–Theorell plots of the interaction between EMAC2005 and RDS1643 on HIV-1 RNase H activity. HIV-1 RT was incubated in the presence of various concentrations of EMAC2005 and in the absence (●) or in the presence of 2.5 (▼), 5 (△), and 10 μM (■) RDS1643.

Table 3. Inhibition of drug-resistant HIV-1 mutated RT-associated functions by EMAC2005.

Compd	IC ₅₀ [μM]			
	Y181C RT		K103N RT	
	RNase H ^[a]	RDDP ^[b]	RNase H ^[a]	RDDP ^[b]
EMAC2005	> 100	8 ± 3	59 ± 8	3 ± 1
efavirenz	–	0.40 ± 0.03	–	0.68 ± 0.05

[a] Compound concentration required to inhibit HIV-1 RT-associated RNase H activity by 50%. [b] Compound concentration required to inhibit HIV-1 RT-associated RDDP activity by 50%.

RNase H activity was almost suppressed, whereas the activity toward the RT-associated RDDP was only slightly affected. This behavior might be explained either by the binding of EMAC2005 to a single site close to Y181, the hydrazones pocket,^[9] or the NNRTIBP, or by the interaction of the compound with two interdependent pockets, the conformations of which are affected by the Y181C mutation.

In silico modeling of the interaction of EMAC2005 with HIV-1 RT

A computational study based on molecular docking experiments in tandem with molecular dynamics simulations was performed to understand the possible mechanism of inhibition of this series of diarylpropenone derivatives. The studies were focused on the most active compound only, that is, EMAC2005.

Molecular docking approaches have become very useful and largely widespread for the prediction of feasible binding modes of a ligand, the target site of which is either known or unknown (blind docking). According to the available literature, dual inhibitory activity could be achieved either by inhibitor

binding into two different sites^[17] or by its binding into a single site.^[7d,8c,9,10c,12] Therefore, we investigated both possibilities.

The very diverse group of NNRTIs bind allosterically in the hydrophobic NNRTIBP and lock the enzyme into an inactive form. Owing to the flexibility of the target and to the different shapes of the known inhibitors (Figure 3a), we decided to perform ensemble docking experiments.^[18] The major conformational changes in the NNRTIBP were taken into account to perform a clustering of the available RT-NNRTI complexes. In particular, the orientation of Y181, Y188, Y183, and primer grip β12–β13 hairpin were considered (Figure 3b).^[19] A representative of each different cluster was picked, and the 3D structure of HIV RT was retrieved from the RCSB Protein Data Bank (PDB).^[20]

QM (quantum mechanical) polarized docking was performed.^[21] This recognition workflow combines docking with semi-empirical methods to calculate charges within the protein environment. This methodology performs significantly better than classical molecular mechanics approaches.^[22] We validated the protocol for this target by performing re-docking experiments (data not shown). The obtained [EMAC2005–RT] complexes were subjected to a post-docking procedure based on energy minimization and successive binding free energy calculations. The binding free energies (ΔG_{bind}) were obtained by applying molecular mechanics and continuum solvation models by using the molecular mechanics generalized Born/surface area (MMGBSA) method.^[23] As reported in Table 4, by comparing the ΔG_{bind} MMGBSA values, we could assert that the most probable binding mode in the NNRTIBP was obtained by docking the compound into the RT conformation model reported in PDB ID 1TV6.^[24]

The best docking pose of EMAC2005 and its comparison with respect to the relative co-crystallized compounds are reported in the Supporting Information (Figures S2–S7). To evalu-

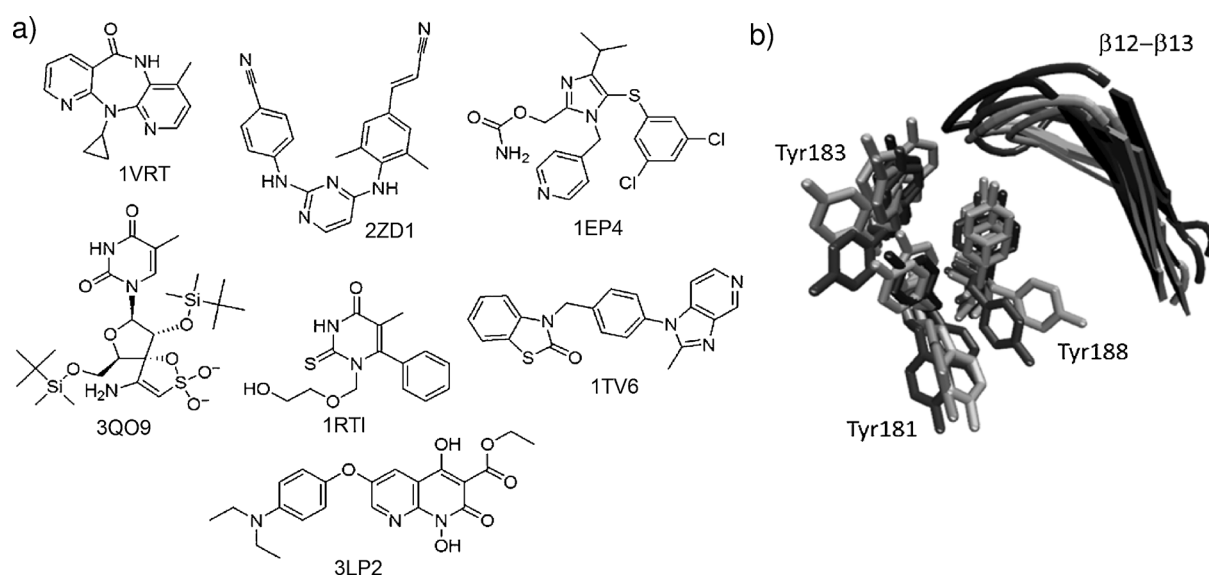


Figure 3. a) Structures and PDB IDs of co-crystallized NNRTIs selected for the ensemble docking procedure. b) Superimposition of the primer grip region and of residues 181, 183, and 188 of employed RT PDB structures for ensemble docking experiments.

Docking site and (box center)	PDB ID	Co-crystallized ligand	G score	ΔG_{bind} MMGBSA
NNRTIBP (center on W229)	1VRT ^[25]	nevirapine	−4.18	−30.6
	2ZD1 ^[26]	rilpivirine	−8.43	−30.7
	1EP4 ^[27]	capravirine	−8.26	−38.8
	3QO9 ^[28]	TSAO-T	−9.21	−35.0
	1RTI ^[25]	HEPT	−11.04	−34.1
	1TV6 ^[24]	CP-94,707	−9.53	−48.0
RNase H domain (center on Q500)	1TV6		−7.50	−38.6
	–	EN37 ^[17]	−5.58	−24.6
RNase H allosteric pocket (center on W229)	3LP2 ^[8c]	MK3	−6.19	−38.4

ate the stability of the complex and the interactions in EMAC2005, we ran a molecular dynamics (MD) simulation up to 6 ns by using Desmond Molecular Dynamics System (version 2.4)^[29] and allowed the whole enzyme free to move into the explicit solvent water environment. Docking and MD simulations were also performed on the mutated enzyme complexes by applying the same protocol described above (docking, energy minimization, ΔG_{bind} MMGBSA calculations, and MD simulations). The best binding mode is depicted in Figure S8. The interaction energy values of the [EMAC2005–RT] complexes are reported in Table 5, whereas their variations, sampled at regular intervals during the simulations over the entire MD trajectory, are illustrated in Figure S9. Furthermore, analysis of the root-mean-square deviation (RMSD), computed onto the RT heavy atoms for the wild-type and mutated enzymes during the MD, showed that the system was structurally stable

Complex	G score	ΔG_{bind} MMGBSA	E_{int} [kcal mol ^{−1}]
NNRTIBP-WT	−9.53	−48.00	−52.01
NNRTIBP-Y181C	−9.90	−44.30	−48.03
NNRTIBP-K103N	−9.59	−45.50	−50.78
allosteric RNaseHIBP-WT	−6.19	−38.40	−40.37
allosteric RNaseHIBP-Y181C	−5.40	−37.10	−38.79
allosteric RNaseHIBP-K103N	−6.06	−36.40	−39.06
SiteQ500	−7.50	−38.60	−42.40

during the simulation (Figure S9).

To assess which binding pocket was responsible for the RNase H inhibitory activity, we considered the described binding pockets: one was located in the catalytic domain and the other was an allosteric site described by Himmel as a hydrazone site^[8c] that was already considered in our previous studies.^[10c,12] The biochemical assay that was directed at verifying the ability of this series of compounds to coordinate the metal ions indicated that the chelation mechanism could be excluded. However, we could not ignore the possibility of a binding site close to the RNase H catalytic residues. Recently, RNase H

inhibitors that bind at a Q507 centered cleft was reported.^[17] Probably, these compounds induce an RNase H domain conformation that prevent this function.

Hence, to include the whole RNase H domain for investigation, in our docking experiments the binding site was defined by a regular box of 97336 Å³ centered on residue Q500. The RT conformational structures adopted for docking experiments were the 1TV6 X-ray structure and the crystallographic model reported in a recent study published by Felts et al., not yet available in the PDB.^[17] In Table 4, the ΔG_{bind} values for the best poses are reported, and in Figure S10, the favorite binding mode is depicted. RMSD and total interaction energy fluctuations during the MD simulations are reported in Figure S11.

Simultaneously, we also investigated whether the RNase H inhibitory activity could depend on the binding into the same allosteric site occupied by hydrazone and naphthyridinone derivatives, described by Himmel.^[8c,9] We found that EMAC2005 showed a similar affinity if bound into the two allosteric sites (Table 4). Furthermore, it was already reported that some compounds that occupy the latter pocket are dual inhibitors. Therefore, we analyzed if binding into this pocket would better explain the dual inhibitory activity of EMAC2005 (Figure S12). In particular, we ran MD simulations by applying the same protocol described above (Figure S13).

According to analysis of the energies of the complexes with the ligand bound in the allosteric binding pocket of RNase H (Table 5 and Figure S14), the obtained interaction energies of EMAC2005 in the wild-type RT and mutated complexes are similar.

Thus, the binding in this allosteric pocket cannot explain the loss of inhibitory activity toward RNase H if Y181 is mutated in cysteine or the decrease in activity if K103 is mutated in asparagine. Consequently, we concluded that the binding of EMAC2005 in this pocket is not the most favored.

Hence, we supposed that polymerase inhibition was due to the binding of EMAC2005 into the NNRTI pocket (Figure 4a). This hypothesis is also supported by the similar behavior of EMAC2005 and CP-94,707 upon testing in the mutated enzymes. In fact, CP-94,707 also acts in the same manner, and both compounds interestingly retain their RDDP activity.^[24] Dif-

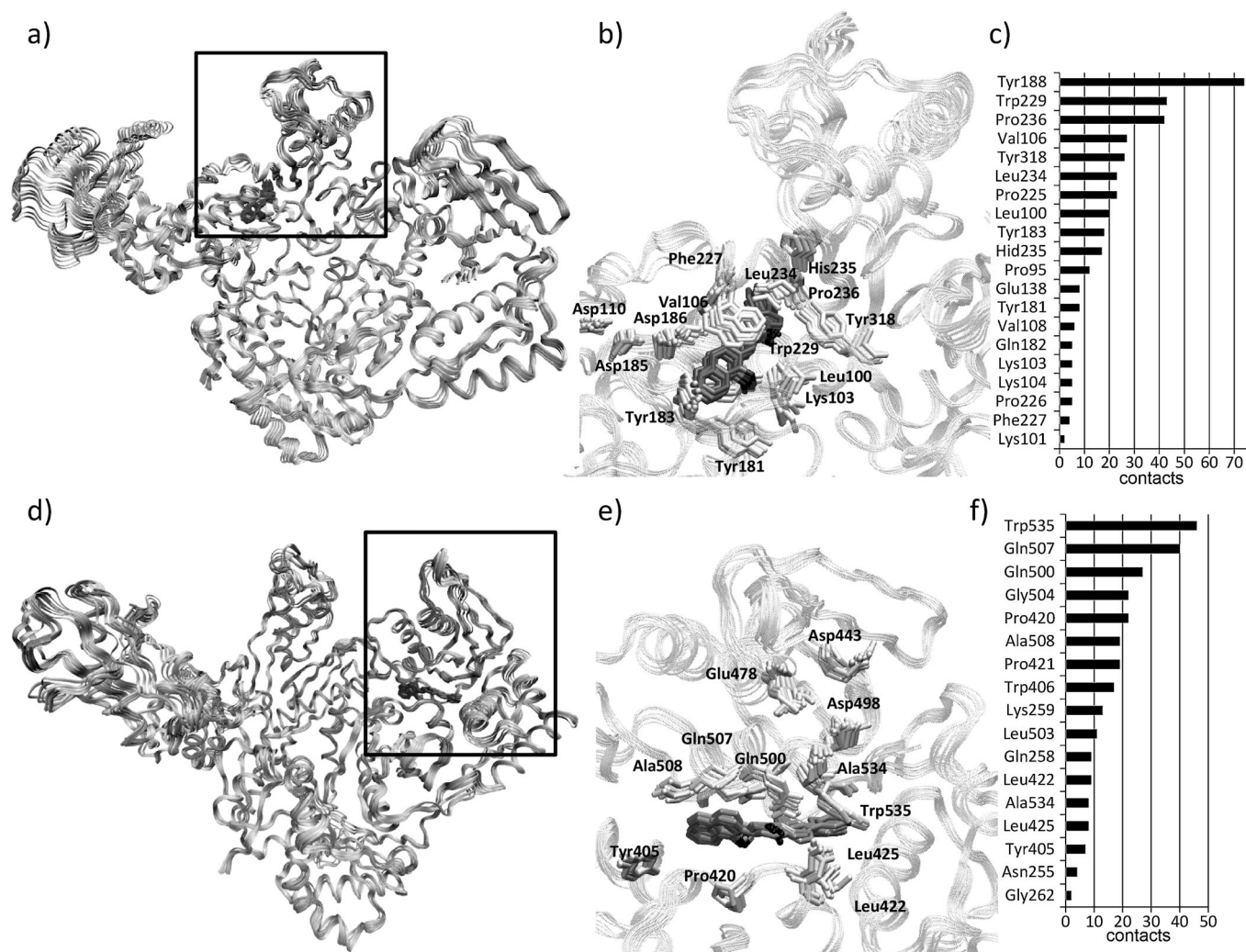


Figure 4. Superimposed structures of 6 ns MD simulation frames of the [EMAC2005–RT] complex: initial, final, and intermediate structure snapshots. a) Overall structure of the HIV-1 RT heterodimer with the NNRTIBP occupied. b) Close-up view of the binding cavity. d) Overall structure of the HIV-1 RT heterodimer with the Q500 site occupied. e) Close-up view of the binding cavity. c,f) Residues involved in the complex stabilization sorted by number of contacts between ligand and receptor. Interacting and catalytic residues are represented as stick structures.

ferently, both biochemical and modeling studies seemed to confirm that binding into an allosteric site close to RNase H catalytic residues was responsible for RNase H inhibitory activity (Figure 4b). To corroborate this hypothesis further, we evaluated the activity of EMAC2005 on A502F RT.^[30] As we expected, this mutation did not affect the RDDP activity. On the contrary, the activity of EMAC2005 on the RNase H function was fivefold lower with respect to that of the wild-type RT, which indicated that residue A502 was involved in the formation of an RNase H allosteric binding pocket in which EMAC2005 could be accommodated.

Still, it remained to be understood why the EMAC2005 inhibitory activity toward RNase H was modified in the mutated enzymes. In this regard, there is considerable evidence that the binding of NNRTIs as well as mutations in the allosteric pocket in the RT DNA polymerase domain affect the activity of the spatially remote RNase H domain. The mechanisms involved in this long-range alteration of RNase H activity are not entirely

understood, but they likely involve changes in the positioning of the RNA/DNA duplex nucleic acid.^[31] Therefore, we examined long-range effects of both mutations by checking the fluctuations of the residues [root-mean-square fluctuation (RMSF)] during MD of the wild-type and mutated enzymes (Figure 5a). We noticed that although the wild-type RT did not show relevant fluctuations in the Q500 site involved in the binding of EMAC2005, some residues in the mutated RTs showed a huge fluctuation that might have disturbed the binding of EMAC2005 (Figure 5b).

Finally, we evaluated the stability of the ternary enzyme–EMAC2005 complex bound in the two allosteric sites (Figure 6). Plots for potential energy and RMSD fluctuations related to the complex are depicted in Figure 6b,c. Analysis showed that the structure reached equilibrium and that the low fluctuations supported the stability of the intermolecular interactions.

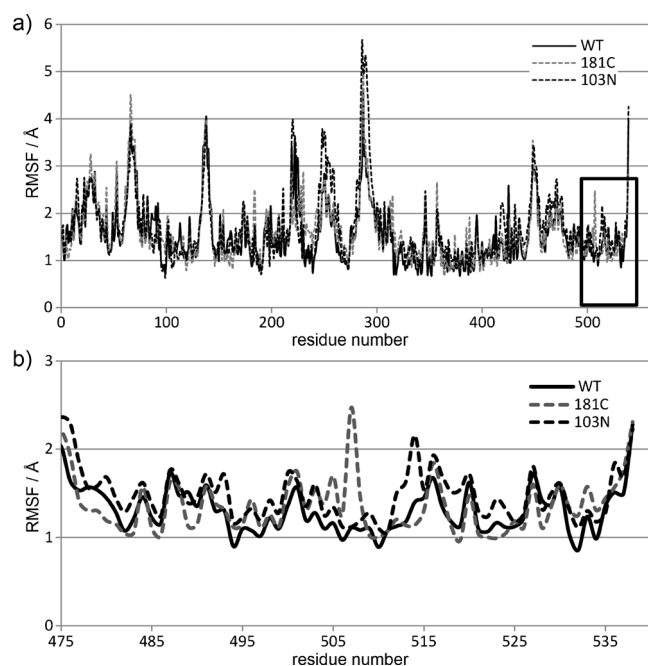


Figure 5. RMSF of subunit p66 during MD. a) Entire wild-type and mutated RT. b) Close-up view of site Q500 residues (boxed region in panel a).

In vitro permeability study of EMAC2005

An in vitro experiment of transmembrane permeation through a biological membrane model was performed to predict the possible interaction of EMAC2005 with a biological membrane, which would thus mimic drug adsorption through a passive diffusion. As shown in Figure 7, the transmembrane permeation profile of EMAC2005 was characterized by a prolonged lag time followed by gradual permeation. This finding was probably due to the fact that the hydrophobic drug has first to diffuse through the aqueous medium and then to interact with the outer hydrophilic layer of the biomembrane model. Only after interaction with the outer biomembrane layer can

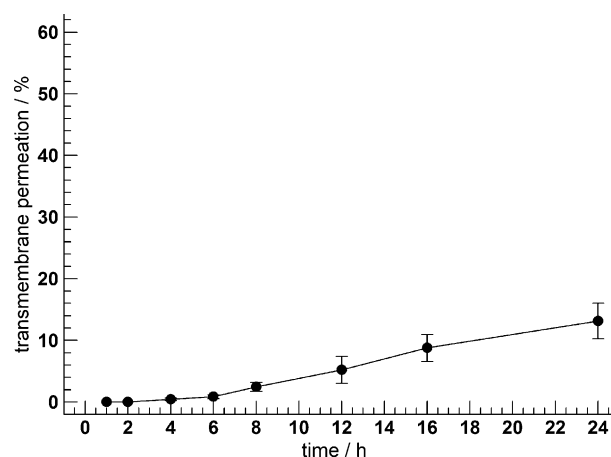


Figure 7. 1. In vitro transmembrane permeation through a biological membrane model of EMAC2005. The experiments were performed at room temperature. Any unapparent error bars are hidden behind the data point; values represent the mean \pm SD of five independent experiments.

EMAC2005 pass through the lipophilic layer, which thus leads to a delay in transmembrane permeation (prolonged lag time). Considering that one of the main factors governing the passive permeation through a biological membrane is the physico-chemical feature of the drug, the elevated hydrophobicity of EMAC2005 could be the reason for the unsuitable transmembrane permeation through the biological membrane model. In fact, the first interaction between the hydrophobic molecule of EMAC2005 and the hydrophilic layer of the biomembrane model may represent the limiting step for easy biological membrane diffusion. This finding seems to be in agreement with other observations^[32] reporting the need for a suitable balance between hydrophilic and hydrophobic features of a molecule to have suitable biological membranes and biological barriers (e.g., blood–brain barrier) passage.

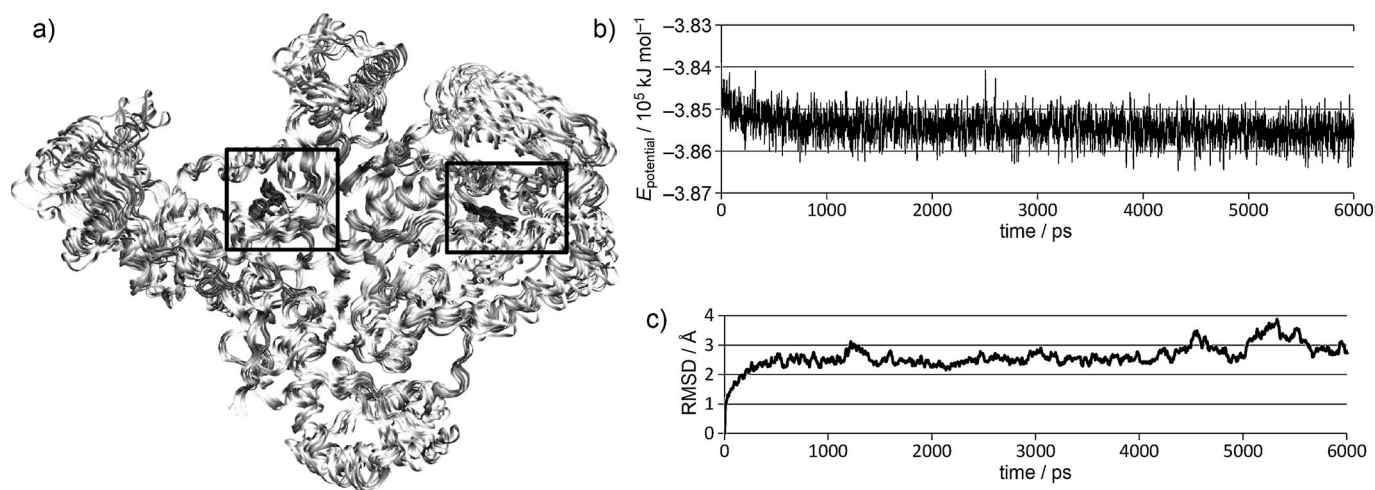


Figure 6. Superimposed structures of 6 ns MD simulation frames of the EMAC2005–RT ternary complex: initial, final, and intermediate structure snapshots. a) Overall structure of the HIV-1 RT heterodimer. b) Potential energy of the complex during the MD simulation. c) RMSD fluctuations during trajectory.

Conclusions

With the aim to obtain dual inhibitors of RT-associated functions, a small series of 1,3-diarylpropenones were designed, synthesized, and tested. The activity of some compounds and the profile toward mutated enzymes was remarkable and suggestive of further modifications and studies. Moreover, investigating the possible mechanism of action of the most-promising compound, that is, EMAC2005, we found that its inhibitory activity could be addressed to the binding at two different enzyme clefts: the NNRTIBP site and an allosteric site close to the RNase H catalytic DEDD motif (site Q500). We highlighted that the compound was better accommodated in a pocket with Y181 and Y188 in close conformation (PDB ID: 1TV6) than in the open conformation of most NNRTIs. This facilitates enzyme recognition if common mutations, such as Y181C and K103N, occur, and therefore, RDDP activity is not impaired. The EMAC2005 binding mode confirms the known key role of W229 and Y188 in the stabilization of the complex. Other interacting residues, namely, L100, P225, L234, Y318, V106, and P236, highlighted the importance of hydrophobic contacts. Instead, most likely, the loss and decrease in RNase H inhibitory potency is due to the improbable entrance of EMAC2005 into the Q500 site if Y181C and K103N mutations occur. This hypothesis was further confirmed by a single-point mutation experiment on the A502 residue. In fact, whereas the inhibition potency of EMAC2005 toward the RDDP function of HIV-1 RT A502F was almost not modified (IC_{50} increased 1.5-fold), the inhibition of the RNase function was remarkably affected with a fivefold decrease in potency. Thus, EMAC2005 most likely behaves as a dual-site dual-function inhibitor.

Experimental Section

Chemistry

Materials and methods: Starting materials and reagents were obtained from commercial suppliers and were used without purification. All melting points were determined by the capillary method with a Stuart SMP11 melting point apparatus or a Büchi-540 capillary melting points apparatus. Melting points, yields of reactions, and the analytical data of the derivatives are reported in Tables S1 and S2. The ^1H NMR spectra of all samples were measured in CDCl_3 at 278.1 K with a Varian Unity 300 spectrometer. In the signal assignments, the chemical shifts of the proton were referenced to the solvent (1H: $\delta=7.24$ ppm). ^{13}C NMR were recorded with a Varian Unity 500 spectrometer by using CDCl_3 as the solvent at 278.1 K. Mass spectra were recorded by using an HPLC-MS/MS Varian (Varian, Palo Alto, CA, USA) system fitted with a 1200 L triple quadrupole mass spectrometer equipped with an electrospray ionization (ESI) source. A Varian MS workstation version 6.8 software was used for data acquisition and processing. Rapid identification was achieved with direct infusion of the purified molecule, dissolved in methanol, on the mass spectrometer source. The ESI mass spectrometer was operated in the positive ion mode. The system was optimized as follows: the electrospray capillary potential was set to 65 V, whereas the shield was set at 725 V. Nitrogen was used as the desolvation solvent gas. The atmospheric pressure ionization (API) housing and drying gas temperatures were kept at 54 and 375 °C, respectively. The scan time was 1 s, and the detector

multiplier voltage was set to 1700 V. Elemental analyses were obtained with a PerkinElmer 240 B microanalyzer. Analytical data of the synthesized compounds are in agreement with the theoretical data. TLC chromatography was performed by using silica gel plates (Merck F₂₅₄), and spots were visualized by UV light.

Synthetic procedures: 1,3-Diarylpropenones were synthesized according to a slightly modified Claisen–Schmidt reaction. Analysis by NMR spectroscopy supported the *E* configuration according to the coupling constants of the double-bond protons that range from 15 to 16 Hz.

Preparation of (*E*)-1-(4-bromophenyl)-3-(1-methoxynaphthalen-2-yl)prop-2-en-1-one (EMAC2000) as a representative procedure: 1-(4-Bromophenyl)ethanone (0.9 g, 4.5 mmol) was dissolved in ethanol (15 mL) and a solution of 10% NaOH was added dropwise at RT. The mixture was stirred for 10 min, and then 1-methoxy-2-naphthaldehyde (1 g, 5.4 mmol) in ethanol solution (15 mL) was added. After 24 h, the reaction was complete (as monitored by TLC, *n*-hexane/ethyl acetate=2:1), and the pale yellow crystalline solid was filtered, washed with water, crystallized with a mixture of water/ethanol, and characterized. Yellow crystals; yield: 67%; mp: 110–112 °C; ^1H NMR (300 MHz, CDCl_3): $\delta=4.06$ (s, 3H, OCH_3), 7.3 (d, $J=9.1$ Hz, 1H, Ar–CH), 7.41 (t, $J=7.5$ Hz, 1H, Ar–CH), 7.55 (t, $J=7.5$ Hz, 1H, Ar–CH), 7.65 (d, $J=8.3$ Hz, 2H, Ar–CH), 7.82 (d, $J=7.5$ Hz, 1H, Ar–CH), 7.85 (d, $J=15.6$ Hz, 1H, –CH=), 7.9 (d, $J=9.0$ Hz, 1H, Ar–CH), 7.93 (d, $J=8.3$ Hz, 2H, Ar–CH), 8.25 (d, $J=8.6$ Hz, 1H, Ar–CH), 8.51 ppm (d, $J=15.6$ Hz, 1H, –CH=); ^{13}C NMR (100 MHz, CDCl_3): $\delta=56.1$ 112.7, 117.1, 123.3, 124.1, 126.6, 127.6, 128.7, 129.0, 130.0, 130.1 (2C), 131.8 (2C), 132.1, 133.1, 137.3, 138.3, 157.2, 190.2 ppm.

(*E*)-1-(4-Fluorophenyl)-3-(1-methoxynaphthalen-2-yl)prop-2-en-1-one (EMAC2001): Yellow crystals; yield: 81%; mp: 93–95 °C; ^1H NMR (300 MHz, CDCl_3): $\delta=4.07$ (s, 3H, OCH_3), 7.11 (t, $J=8.5$ Hz, 1H, Ar–CH), 7.26 (d, $J=9.1$ Hz, 2H, Ar–CH), 7.42 (d, $J=7.1$ Hz, 1H, Ar–CH), 7.50 (t, $J=8.5$ Hz, 1H, Ar–CH), 7.57 (d, $J=7.1$ Hz, 1H, Ar–CH), 7.78 (d, $J=15.9$ Hz, 1H, –CH=), 7.93 (d, $J=8.6$ Hz, 1H, Ar–CH), 8.09 (t, $J_{\text{H,H}}=9.1$ Hz, $J_{\text{H,F}}=9.3$ Hz, 2H, Ar–CH), 8.18 (d, $J=8.5$ Hz, 1H, Ar–CH), 8.43 ppm (d, 1H, $J=15.9$ Hz, –CH=); ^{13}C NMR (100 MHz, CDCl_3): $\delta=56.5$, 112.7, 115.7, 123.3, 124.0, 126.8, 127.6, 128.6 (2C), 129.0, 130.0 (2C), 131.1, 131.3, 132.0, 133.0, 136.2, 138.3, 157.2, 190.0 ppm.

(*E*)-1-(4-Methoxyphenyl)-3-(1-methoxynaphthalen-2-yl)prop-2-en-1-one (EMAC2002): Yellow crystals; yield: 83%; mp: 137–139 °C; ^1H NMR (300 MHz, CDCl_3): $\delta=3.9$ (s, 3H, OCH_3), 4.05 (s, 3H, OCH_3), 7.00 (d, $J=8.9$ Hz, 1H, Ar–CH), 7.33 (d, $J=9.0$ Hz, 2H, Ar–CH), 7.70 (t, $J=8$ Hz, 1H, Ar–CH), 7.47 (d, $J=16.0$ Hz, 1H, –CH=), 7.55 (t, $J=8$ Hz, 1H, Ar–CH), 7.82 (d, $J=8.0$ Hz, 1H, Ar–CH), 7.89 (d, $J=9.0$ Hz, 1H, Ar–CH), 8.08 (d, $J=9.0$ Hz, 1H, Ar–CH), 8.28 (d, $J=9.0$ Hz, 2H, Ar–CH), 8.45 (d, $J=16.0$ Hz, 1H, –CH=); ^{13}C NMR (100 MHz, CDCl_3): $\delta=55.4$, 56.5, 112.7, 113.5, 117.7, 123.5, 124.1, 127.2, 127.6, 128.6, 129.1, 130.9 (2C), 131.5 (2C), 131.7, 133.1, 137.0, 156.9, 163.3, 189.5 ppm.

(*E*)-1-(4-Chlorophenyl)-3-(1-methoxynaphthalen-2-yl)prop-2-en-1-one (EMAC2003): Yellow crystals; yield: 53%; mp: 108–109 °C; ^1H NMR (300 MHz, CDCl_3): $\delta=4.06$ (s, 3H, OCH_3), 7.33 (d, $J=9.1$ Hz, 1H, Ar–CH), 7.41 (t, $J=7.8$ Hz, 1H, Ar–CH), 7.49 (d, $J=8.4$ Hz, 2H, Ar–CH), 7.53 (d, $J=15.6$ Hz, 1H, –CH=), 7.55 (t, $J=7.8$ Hz, 1H, Ar–CH), 7.74 (d, $J=8.1$ Hz, 1H, Ar–CH), 7.90 (d, $J=9.6$ Hz, 1H, Ar–CH), 8.01 (d, $J=8.3$ Hz, 2H, Ar–CH), 8.25 (d, $J=8.6$ Hz, 1H, Ar–CH), 8.51 ppm (d, $J=15.6$ Hz, 1H, –CH=); ^{13}C NMR (500 MHz, CDCl_3): $\delta=56.3$, 112.7, 117.1, 123.3, 124.0, 126.7, 127.6, 128.6, 128.8 (2C),

129.0, 130.0 (2C), 132.1, 133.1, 136.9, 138.3, 139.0, 157.2, 190.0 ppm.

(E)-1-(3-Nitrophenyl)-3-(1-methoxynaphthalen-2-yl)prop-2-en-1-one (EMAC2004): Pale orange crystals; yield: 64%; mp: 143–145 °C; ¹H NMR (300 MHz, CDCl₃): δ = 4.10 (s, 3H, OCH₃), 7.35 (d, *J* = 8.9 Hz, 1H, Ar–CH), 7.42 (t, *J* = 7.8 Hz, 1H, Ar–CH), 7.58 (t, *J* = 8.5 Hz, 1H, Ar–CH), 7.72 (t, *J* = 7.8 Hz, 1H, Ar–CH), 7.83 (d, *J* = 8.0 Hz, 1H, Ar–CH), 7.93 (d, *J* = 8.5 Hz, 1H, Ar–CH), 7.94 (d, *J* = 15.6 Hz, 1H, –CH=), 8.25 (d, *J* = 8.5 Hz, 1H, Ar–CH), 8.39 (d, *J* = 8.5 Hz, 1H, Ar–CH), 8.44 (d, *J* = 8.0 Hz, 1H, Ar–CH), 8.60 (d, *J* = 15.6 Hz, <1H, C–>CH=), 8.89 ppm (s, 1H, Ar–CH); ¹³C NMR (500 MHz, CDCl₃): δ = 56.3, 112.6, 116.6, 123.1, 123.4, 124.1, 125.7, 126.8, 127.8, 128.8, 129.0, 129.8, 132.7, 133.1, 134.1, 139.5, 140.0, 148.3, 157.6, 189.0 ppm.

(E)-1-(4-Biphenyl)-3-(1-methoxynaphthalen-2-yl)prop-2-en-1-one (EMAC2005): Yellow crystals; yield: 87%; mp: 104–105 °C; ¹H NMR (300 MHz, CDCl₃): δ = 4.07 (s, 3H, OCH₃), 7.34–7.50 (m, 2H, Ar–CH), 7.56 (t, *J* = 8.1 Hz, 1H, Ar–CH), 7.69 (d, *J* = 7.8 Hz, 2H, Ar–CH), 7.75 (d, *J* = 7.8 Hz, 2H, Ar–CH), 7.83 (d, *J* = 8.8 Hz, 1H, Ar–CH), 7.88 (d, *J* = 8.0 Hz, 1H, Ar–CH), 7.91 (d, *J* = 8.2 Hz, 2H, Ar–CH), 7.95 (d, *J* = 15.9 Hz, 1H, –CH=), 8.04 (d, *J* = 8.2 Hz, 2H, Ar–CH), 8.19 (d, *J* = 8.8 Hz, 1H, Ar–CH), 8.29 (d, *J* = 8.1 Hz, 1H, Ar–CH), 8.54 ppm (d, *J* = 15.9 Hz, 1H, –CH=); ¹³C NMR (100 MHz, CDCl₃): δ = 56.4, 112.8, 117.4, 123.5, 124.0, 127.2 (3C), 127.3 (3C), 127.5, 128.1, 128.6, 128.9 (2C), 129.1, 129.2 (2C), 131.8, 137.3, 137.7, 140.1, 145.3, 157.1, 190.7 ppm.

Biology

Protein expression and purification: The recombinant HIV-1 RT protein, the coding gene of which was subcloned in the p6HRT_prot plasmid, was expressed in *E. coli* strain M15.^[33] The bacteria cells were grown up to an optical density (at 600 nm) of 0.8 and induced with 1.7 mM isopropyl β-D-1-thiogalactopyranoside (IPTG) for 5 h. HIV-1 RT purification was performed as described.^[8h] Briefly, cell pellets were re-suspended in lysis buffer (20 mM HEPES, pH 7.5; 0.5 M NaCl; 5 mM β-mercaptoethanol; 5 mM imidazole; 0.4 mg mL⁻¹ lysozyme), incubated on ice for 20 min, sonicated, and centrifuged at 30000 g for 1 h. The supernatant was applied to a His-binding resin column and washed thoroughly with wash buffer (20 mM HEPES, pH 7.5; 0.3 M NaCl; 5 mM β-mercaptoethanol; 60 mM imidazole; 10% glycerol). RT was eluted by imidazole gradient, and the enzyme-containing fractions were pooled and dialyzed and aliquots were stored at –80 °C.

RNase H polymerase-independent cleavage assay: The HIV-1 RT-associated RNase H activity was measured as described^[12] in 100 μL reaction volume containing 50 mM Tris HCl, pH 7.8; 6 mM MgCl₂; 1 mM dithiothreitol (DTT); 80 mM KCl; hybrid RNA/DNA (5'-GTT TTC TTT TCC CCC CTG AC-3'-fluorescein; 5'-CAA AAG AAA AGG GGG GAC UG-3'-dabcyl) and 3.8 nM RT. The reaction mixture was incubated for 1 h at 37 °C. The enzymatic reaction was stopped with the addition of ethylenediaminetetraacetic acid (EDTA) and measured with a Victor3 instrument (Perkin) at 490/528 nm.

DNA polymerase assay: The HIV-1 RT-associated (RDDP) activity was measured by using an Invitrogen EnzCheck Reverse Transcriptase Assay Kit, in 50 μL volume containing 60 mM Tris HCl, pH 8.1; 8 mM MgCl₂; 60 mM KCl; 13 mM DTT; 100 μM dTTP; 2 nM HIV-1 RT; poly(A)-oligo(dT). The reaction mixture was incubated for 30 min at 37 °C. The enzymatic reaction was stopped with the addition of EDTA and measured with Victor3 (Perkin) at 502/523 nm after the addition of picogreen.

Cell lines and virus: The human embryonic c kidney cells 293T and the human T-lymphoid Jurkat cell line (clone E6-1) were from the American Type Culture Collection and maintained in DMEM or RPMI medium (Invitrogen), respectively, containing 10% fetal bovine serum (FBS, Invitrogen), at 37 °C under a humidified 5% CO₂ atmosphere. Recombinant viral stock was produced by transient transfection of 293T cells as previously described^[34] and used to transduce Jurkat cells. In this context, an *env*-defective provirus encoding the bacterial chloramphenicol acetyltransferase (CAT) gene was complemented in *trans* by the envelope glycoprotein derived from the laboratory-adapted T-cell-tropic strain HXBc2. The level of CAT expression in the infected cells reflects the efficiency of a single round of the retroviral infection cycle.

Cytotoxicity assay: For cytotoxicity assays, cell lines were seeded in 96-well plates (Falcon) at an initial density of 10⁵ cells per 100 μL in medium containing 10% FBS, in the absence or presence of serial dilutions of test compounds. Plates were incubated for 72 h at 37 °C in under a humidified 5% CO₂ atmosphere. Cell viability was determined by using Cell Proliferation Kit I (MTT) (Roche).

Molecular modeling

Ligand preparation: Theoretical 3D models of the most active derivative EMAC2005 was built by means of Maestro.^[35] The inhibitor structure was optimized by means of an energy minimization performed by using the MMFFs force field,^[36] the GB/SA^[37] water implicit solvation model, and the Polak–Ribier Conjugate Gradient (PRCG) method by converging on gradient with a threshold of 0.05 kJ (mol Å)⁻¹.

Protein preparation: The coordinates for reverse transcriptase enzymes were taken from the RCSB Protein Data Bank^[20] (PDB IDs: 1VRT,^[25] 2ZD1,^[26] 1EP4,^[27] 3QO9,^[28] 1RTI,^[25] 1TV6,^[24] and 3LP2).^[8c] The proteins were prepared by using the Maestro Protein Preparation Wizard. Original water molecules were removed and termini were capped. The bond orders and formal charges were added for hetero groups, and all the hydrogen atoms were added in the structure. Missing atoms and residues were included. After preparation, the structures were refined to optimize the hydrogen-bond network by using OPLS_2005^[38] force field. The minimization was terminated once the energy converged or the RMSD reached a maximum cutoff of 0.30 Å.

Docking protocol: Molecular docking studies were performed by using the QMPL workflow protocol.^[21] Grids were defined around the refined structure by centering on the residue indicated in Table 3 and fixing the box volume at 97336 Å³. The extra precision (XP) docking algorithm was applied for scoring theoretical poses. The other settings were left as default. The same protocol was applied for all the simulations indicated in Tables 3 and 4.

Post-docking protocol: A total of 10000 steps of the Polak–Ribier conjugate gradient (PRCG) minimization method were conducted on the top-ranked theoretical complexes by using the OPLS_2005 force field. The optimization process was performed up to the derivative convergence criterion equal to 0.01 kJ (mol Å)⁻¹. The binding free energies (ΔG_{bind}) were computed by applying molecular mechanics and continuum solvation models with the molecular mechanics generalized Born/surface area (MMGBSA) method.^[23]

Best docking complexes were submitted to 6 ns of MD by using Desmond (version 2.4).^[39] The complexes were solvated with a TIP3P (transferable intermolecular potential 3-Point)^[40] box of water and counter ions were added to neutralize the system net charge. The solvated models were optimized, and subsequently

the MTK_NPT (Martyna–Tobias–Klein with constant number of particles, pressure and temperature) ensemble was employed.^[41] The default stages in the relaxation process for the NPT ensemble included two energy minimizations and four simulation steps. During the energy minimizations, two runs of 2000 iteration were processed by using the steepest descent method: during the first run, the protein structure was fixed by a force restraint constant of 50 kcal(molÅ)⁻¹, and in the second run all restraints were removed. With the first simulation, at NVT (constant number of particles, volume, and temperature) ensemble, the system reached a temperature of 10 K. In the following three simulations in the NPT ensemble, the system was heated up to 300 K and the pressure was kept constant at 100 kPa by using the Berendsen thermostat–barostat. During the production phase, temperature and pressure were kept constant by using the Nosè–Hoover thermostat–barostat. The energy and trajectory were recorded every 1.2 and 4.8 ps, respectively. For multiple time step integration, a RESPA (reversible reference system propagator algorithm)^[42] was applied to integrate the equation of motion with Fourier-space electrostatics computed every 6 fs, and all remaining interactions computed every 2 fs. All chemical bond lengths involving hydrogen atoms were fixed with SHAKE.^[43] The short-range cutoff was set to 9 Å, and the smooth particle mesh Ewald method (PME)^[44] was used for long-range electrostatic interactions. The resulting seven trajectories were analyzed in terms of interaction energies and geometries. The same protocol was applied for the EMAC2005–RT ternary complex. Molecular modeling figures were depicted by LigandScout^[45] and VMD (version 1.8.7).^[46]

In vitro membrane permeation studies

HPLC determination of EMAC2005: The sensitive HPLC method with UV detection was developed for the quantitative determination of EMAC2005. The chromatographic system was a HPLC Jasco model PU-1580 (Tokyo, Japan) with a 20 µL loop injection valve. The chromatographic system was equipped with a Jasco MD 1510 diode array detector, which was set at $\lambda_{\max}=296$ for EMAC2005. The separation was performed by using a C18 reverse-phase Phenomenex column (Jupiter 250×4.60 mm, 5 µm particle size), which was maintained at room temperature. The mobile phase was pH 9 water (eluent A) and acetonitrile (eluent B) and it was delivered at a flow rate of 1 mL min⁻¹. Solvents were degassed by sonication for 15 min. A gradient elution method was applied for the determination of EMAC2005. The gradient was set as follows: eluent A/eluent B = 70:30, 0–7 min; linear increase of eluent B to 60%, 7–9 min; linear increase of eluent B to 70%, 9–12 min; eluent A/eluent B = 30:70, 12–19 min; linear decrease of eluent B to 50%, 19–21 min; and then the system was linearly returned to the original conditions, 21–25 min (see the Supporting Information for further details). HPLC data were processed by using the Borwin chromatography software (version 1.5) from Jasco. A pure ethanol solution of EMAC2005 was prepared (1 mg mL⁻¹) and used as a stock solution for the calibration curve. EMAC2005 quantification was performed by using a calibration curve in a linear concentration interval ranging from 0.1 to 100 µg mL⁻¹, according to Equation (1):

$$\text{AUC} = 0.5598x - 1.94010 \quad (1)$$

in which AUC is the area under the curve (mAu×min) and x is the drug concentration (µg mL⁻¹).

In vitro transmembrane permeation: A model of biological membrane was prepared as elsewhere reported.^[47] Briefly, a poly-

carbonate membrane (50 nm pore size) was presoaked in pH 7.4 isotonic phosphate buffer for 3 h and layered on a synthetic cellulose nitrate membrane (molecular weight cutoff = 10000 Da), which was previously impregnated with a liquid paraffin/lauryl alcohol (2.1:10 w/w) mixture up to the doubling of the weight. Flow Franz diffusion cells were used for the transmembrane permeation of EMAC2005, and they were characterized by a surface area of 0.75 cm² and a nominal receiving volume of 4.75 mL. The model of biological membrane was placed horizontally between the donor and receptor compartments. An ethanol/water mixture (50:50 v/v) was used to fill the receptor compartment. The same mixture (200 µL) was used to suspend the drug. This suspension was placed into the donor compartments. The receptor fluid was constantly stirred at 600 rpm during the experiments by means of a magnetic anchor and warmed (GR 150 thermostat, Grant Instruments Ltd, Cambridge, UK) to 37 °C. These conditions were maintained throughout the experiments. At predetermined times, 400 µL of the receptor compartment was withdrawn by using a Minipuls 3 peristaltic pump [Gilsen Italia S.r.l., Cinisello Balsamo (MI), Italy] connected to a FC 204 fraction collector [Gilsen Italia S.r.l., Cinisello Balsamo (MI), Italy] and immediately replaced with the same volume of fresh solution. The amount of EMAC2005 that permeated through the membranes was immediately analyzed by HPLC. Experiments were performed in triplicate, and results are the mean ± SD of five different experiments.

Acknowledgements

This work was supported by RAS (Regione Autonoma della Sardegna) grant LR 7/2007 CRP2 450, CRP-24915 and Istituto Superiore di Sanità grant RF-PAD-2009-1304305 n.40H98. The PhD grant of R.M. was funded by Fondazione Banco di Sardegna. F.E. was supported by RAS fellowships, co-financed with funds from PO Sardinia FSE 2007–2013 and of LR 7/2007, project CRP2 683.

Keywords: antiviral agents · dual inhibitors · enzymes · HIV-1 · molecular modeling · RNase H

- [1] a) P. Zhan, X. Liu, Z. Li, C. Pannecouque, E. De Clercq, *Curr. Med. Chem.* **2009**, *16*, 3903–3917; b) R. Morphy, Z. Rankovic, *J. Med. Chem.* **2005**, *48*, 6523–6543.
- [2] B. L. Roth, D. J. Sheffler, W. K. Kroeze, *Nat. Rev. Drug Discovery* **2004**, *3*, 353–359.
- [3] Y. Mehellou, E. De Clercq, *J. Med. Chem.* **2010**, *53*, 521–538.
- [4] G. N. Nikolenko, S. Palmer, F. Maldarelli, J. W. Mellors, J. M. Coffin, V. K. Pathak, *Proc. Natl. Acad. Sci. USA* **2005**, *102*, 2093–2098.
- [5] F. Esposito, A. Corona, E. Tramontano, *Mol. Biol. Int.* **2012**, 586401.
- [6] O. Schatz, F. V. Cromme, F. Grüninger-Leitch, S. F. J. Le Grice, *FEBS Lett.* **1989**, *257*, 311–314.
- [7] a) K. Klumpp, T. Mirzadegan, *Curr. Pharm. Des.* **2006**, *12*, 1909–1922; b) E. Tramontano, *Mini-Rev. Med. Chem.* **2006**, *6*, 727–737; c) E. Tramontano, R. Di Santo, *Curr. Med. Chem.* **2010**, *17*, 2837–2853; d) S. Distinto, E. Maccioni, R. Meleddu, A. Corona, S. Alcaro, E. Tramontano, *Curr. Pharm. Des.* **2013**, *19*, 1850–1859.
- [8] a) J. Q. Hang, S. Rajendran, Y. Yang, Y. Li, P. W. K. In, H. Overton, K. E. B. Parkes, N. Cammack, J. A. Martin, K. Klumpp, *Biochem. Biophys. Res. Commun.* **2004**, *317*, 321–329; b) E. Tramontano, F. Esposito, R. Badas, R. Di Santo, R. Costi, P. La Colla, *Antiviral Res.* **2005**, *65*, 117–124; c) D. M. Himmel, K. A. Maegley, T. A. Pauly, J. D. Bauman, K. Das, C. Dharia, A. D. Clark, Jr., K. Ryan, M. J. Hickey, R. A. Love, S. H. Hughes, S. Bergqvist, E. Arnold, *Structure* **2009**, *17*, 1625–1635; d) T. A. Kirschberg, M. Balakrishnan, N. H. Squires, T. Barnes, K. M. Brenda, X. Chen, E. J. Eisenberg, W. Jin, N. Kutty, S. Leavitt, A. Licican, Q. Liu, X. Liu, J. Mak, J. K. Perry, M. Wang, W. J. Watkins, E. B. Lansdon, *J. Med. Chem.* **2009**, *52*,

- 5781–5784; e) H.-P. Su, Y. Yan, G. S. Prasad, R. F. Smith, C. L. Daniels, P. D. Abeywickrema, J. C. Reid, H. M. Loughran, M. Kornienko, S. Sharma, J. A. Grobler, B. Xu, V. Sardana, T. J. Allison, P. D. Williams, P. L. Darke, D. J. Hazuda, S. Munshi, *J. Virol.* **2010**, *84*, 7625–7633; f) S. Chung, D. M. Himmel, J.-K. Jiang, K. Wojtak, J. D. Bauman, J. W. Rausch, J. A. Wilson, J. A. Beutler, C. J. Thomas, E. Arnold, S. F. J. Le Grice, *J. Med. Chem.* **2011**, *54*, 4462–4473; g) E. B. Lansdon, Q. Liu, S. A. Leavitt, M. Balakrishnan, J. K. Perry, C. Lancaster-Moyer, N. Kutty, X. Liu, N. H. Squires, W. J. Watkins, T. A. Kirschberg, *Antimicrob. Agents Chemother.* **2011**, *55*, 2905–2915; h) V. Suchaud, F. Bailly, C. Lion, E. Tramontano, F. Esposito, A. Corona, F. Christ, Z. Debyser, P. Cotellet, *Bioorg. Med. Chem. Lett.* **2012**, *22*, 3988–3992.
- [9] D. M. Himmel, S. G. Sarafianos, S. Dharmasena, M. M. Hossain, K. McCoy-Simandle, T. Iliina, A. D. Clark, J. L. Knight, J. G. Julias, P. K. Clark, K. Krogh-Jespersen, R. M. Levy, S. H. Hughes, M. A. Parniak, E. Arnold, *ACS Chem. Biol.* **2006**, *1*, 702–712.
- [10] a) T. Kharlamova, F. Esposito, L. Zinzula, G. Floris, Y.-C. Cheng, G. Dutschman, E. Tramontano, *Med. Chem.* **2009**, *5*, 398–410; b) E. Tramontano, T. Kharlamova, L. Zinzula, F. Esposito, *J. Chemother.* **2011**, *23*, 273–276; c) F. Esposito, T. Kharlamova, S. Distinto, L. Zinzula, Y.-C. Cheng, G. Dutschman, G. Floris, P. Markt, A. Corona, E. Tramontano, *FEBS J.* **2011**, *278*, 1444–1457.
- [11] F. Esposito, A. Corona, L. Zinzula, T. Kharlamova, E. Tramontano, *Chemotherapy* **2012**, *58*, 299–307.
- [12] S. Distinto, F. Esposito, J. Kirchmair, M. C. Cardia, M. Gaspari, E. Maccioni, S. Alcaro, P. Markt, G. Wolber, L. Zinzula, E. Tramontano, *Eur. J. Med. Chem.* **2012**, *50*, 216–229.
- [13] L. M. A. Lima, E. J. Barreiro, *Curr. Med. Chem.* **2005**, *12*, 23–49.
- [14] H. Pelemans, R. Esnouf, E. De Clercq, J. Balzarini, *Mol. Pharmacol.* **2000**, *57*, 954–960.
- [15] T. Rosen, A. A. Nagel, J. P. Rizzi, J. L. Ives, J. B. Daffeh, A. H. Ganong, K. Guarino, J. Heym, S. McLean, *J. Med. Chem.* **1990**, *33*, 2715–2720.
- [16] T. Yonetani, *Methods Enzymol.* **1982**, *87*, 500–509.
- [17] A. K. Felts, K. LaBarge, J. D. Bauman, D. V. Patel, D. M. Himmel, E. Arnold, M. A. Parniak, R. M. Levy, *J. Chem. Inf. Model.* **2011**, *51*, 1986–1998.
- [18] S.-Y. Huang, X. Zou, *Proteins: Struct. Funct. Bioinf.* **2007**, *66*, 399–421.
- [19] K. A. Paris, O. Haq, A. K. Felts, K. Das, E. Arnold, R. M. Levy, *J. Med. Chem.* **2009**, *52*, 6413–6420.
- [20] H. M. Berman, J. Westbrook, Z. Feng, G. Gilliland, T. N. Bhat, H. Weissig, I. N. Shindyalov, P. E. Bourne, *Nucleic Acids Res.* **2000**, *28*, 235–242.
- [21] Schrödinger LLC, “QM Polarized Protocol” in *Schrödinger Suite*, New York, NY, USA.
- [22] J. Y. Chung, J.-M. Hah, A. E. Cho, *J. Chem. Inf. Model.* **2009**, *49*, 2382–2387.
- [23] P. A. Kollman, I. Massova, C. Reyes, B. Kuhn, S. Huo, L. Chong, M. Lee, T. Lee, Y. Duan, W. Wang, O. Donini, P. Cieplak, J. Srinivasan, D. A. Case, T. E. Cheatham, *Acc. Chem. Res.* **2000**, *33*, 889–897.
- [24] J. D. Pata, W. G. Stirtan, S. W. Goldstein, T. A. Steitz, *Proc. Natl. Acad. Sci. USA* **2004**, *101*, 10548–10553.
- [25] J. S. Ren, R. Esnouf, E. Garman, D. Somers, C. Ross, I. Kirby, J. Keeling, G. Darby, Y. Jones, D. Stuart, D. Stammers, *Nat. Struct. Biol.* **1995**, *2*, 293–302.
- [26] K. Das, J. D. Bauman, A. D. Clark, Y. V. Frenkel, P. J. Lewi, A. J. Shatkin, S. H. Hughes, E. Arnold, *Proc. Natl. Acad. Sci. USA* **2008**, *105*, 1466–1471.
- [27] J. S. Ren, C. Nichols, L. E. Bird, T. Fujiwara, H. Sugimoto, D. I. Stuart, D. K. Stammers, *J. Biol. Chem.* **2000**, *275*, 14316–14320.
- [28] K. Das, J. D. Bauman, A. S. Rim, C. Dharia, A. D. Clark, M.-J. Camarasa, J. Balzarini, E. Arnold, *J. Med. Chem.* **2011**, *54*, 2727–2737.
- [29] K. J. Bowers, E. Chow, H. Xu, R. O. Dror, M. P. Eastwood, B. A. Gregersen, J. L. Klepeis, I. Kolossvary, M. A. Moraes, F. D. Sacerdoti, J. K. Salmon, Y. Shan, D. E. Shaw in *Proceedings SC06 ACM/IEEE Conference*, Tampa, FL (USA), **2006**, p. 84.
- [30] Q. Gong, L. Menon, T. Iliina, L. G. Miller, J. Ahn, M. A. Parniak, R. Ishima, *Chem. Biol. Drug Des.* **2011**, *77*, 39–47.
- [31] a) J. M. Seckler, M. D. Barkley, P. L. Wintrod, *Biophys. J.* **2011**, *100*, 144–153; b) T. Iliina, K. LaBarge, S. G. Sarafianos, R. Ishima, M. A. Parniak, *Biology* **2012**, *1*, 521–541.
- [32] C. Celia, D. Cosco, D. Paolino, M. Fresta, *Med. Res. Rev.* **2011**, *31*, 716–756.
- [33] a) E. Tramontano, Y. c. Cheng, *Biochem. Pharmacol.* **1992**, *43*, 1371–1376; b) J. W. Mellors, G. J. Im, E. Tramontano, S. R. Winkler, D. J. Medina, G. E. Dutschman, H. Z. Bazmi, G. Piras, C. J. Gonzalez, Y. C. Cheng, *Mol. Pharmacol.* **1993**, *43*, 11–16.
- [34] C. Parolin, B. Gatto, C. Del Vecchio, T. Pecere, E. Tramontano, V. Cecchetti, A. Fravolini, S. Masiero, M. Palumbo, G. Palù, *Antimicrob. Agents Chemother.* **2003**, *47*, 889–896.
- [35] Schrödinger LLC, *Maestro GUI*, New York, NY, USA, **2012**.
- [36] T. Halgren, *J. Comput. Chem.* **1996**, *17*, 520–552.
- [37] W. Hasel, T. F. Hendrickson, W. C. Still, *Tetrahedron Comput. Methodol.* **1988**, *1*, 103–116.
- [38] G. A. Kaminski, R. A. Friesner, J. Tirado-Rives, W. L. Jorgensen, *J. Phys. Chem. B* **2001**, *105*, 6474–6487.
- [39] K. J. Bowers, R. O. Dror, D. E. Shaw, *J. Chem. Phys.* **2006**, *124*, 184109–184111.
- [40] W. L. Jorgensen, J. Chandrasekhar, J. D. Madura, R. W. Impey, M. L. Klein, *J. Chem. Phys.* **1983**, *79*, 926–935.
- [41] G. J. Martyna, D. J. Tobias, M. L. Klein, *J. Chem. Phys.* **1994**, *101*, 4177–4189.
- [42] D. A. Gibson, E. A. Carter, *J. Phys. Chem.* **1993**, *97*, 13429–13434.
- [43] J.-P. Ryckaert, G. Ciccotti, H. Berendsen, *J. Comp. Physiol.* **1977**, *23*, 327–341.
- [44] T. Darden, D. York, L. Pedersen, *J. Chem. Phys.* **1993**, *98*, 10089–10092.
- [45] a) IntelLigand Software GmbH, *LigandScout 3.0*, Maria Enzersdorf, Austria, **2009**; b) G. Wolber, T. Langer, *J. Chem. Inf. Model.* **2005**, *45*, 160–169.
- [46] W. Humphrey, A. Dalke, K. Schulten, *J. Mol. Graphics* **1996**, *14*, 33–38.
- [47] G. Cavallaro, M. Fresta, G. Giammona, G. Puglisi, A. Villari, *Int. J. Pharm.* **1994**, *111*, 31–41.

Received: February 6, 2014

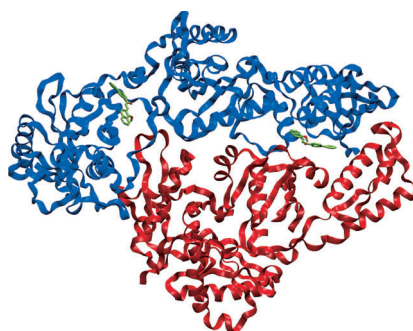
Published online on ■ ■ ■■, 0000

FULL PAPERS

R. Meleddu, V. Cannas, S. Distinto,*
G. Sarais, C. Del Vecchio, F. Esposito,
G. Bianco, A. Corona, F. Cottiglia,
S. Alcaro, C. Parolin, A. Artese, D. Scalise,
M. Fresta, A. Arridu, F. Ortuso,
E. Maccioni,* E. Tramontano



**Design, Synthesis, and Biological
Evaluation of 1,3-Diarylpropenones as
Dual Inhibitors of HIV-1 Reverse
Transcriptase**



1,3-Diarylpropenones were synthesized and assayed for their activity toward HIV-1 reverse transcriptase (RT). Dual inhibition properties in the low-micromolar range were observed, and mutations in the RT binding pocket were found to have an interesting effect on inhibition. Biochemical and computational approaches were applied with an aim to understand the possible mechanism of action.